CONDENSED MATTER: STRUCTURE, MECHANICAL AND THERMAL PROPERTIES

Neutron Diffraction Measurements of a Thermally Fatigued Single Crystal Superalloy

CHIN. PHYS. LETT. Vol. 26, No. 8 (2009) 086201

Neutron Diffraction Measurements of a Thermally Fatigued Single Crystal Superalloy

SUN Guang-Ai(孙光爱)[1,2**], CHEN Bo(陈波)[1,2], WU Er-Dong(吴二冬)[3], LI Jin-Chao(李金超)[3], T. Pirling[4], D. Hughes[4]

[1]*Institute of Atomic and Molecular Physics, Sichuan University, Chengdu 610065*
[2]*Institute of Nuclear Physics and Chemistry, Mianyang 621900*
[3]*National Laboratory for Materials Science, IMR CAS, Shenyang 110016*
[4]*Institute of Laue Langevin, Grenoble 38042, France*

(Received 30 April 2009)

The thermally fatigued single crystal superalloy DZ125L is investigated by neutron diffraction measurements. The measurements, made using the φ angle oscillating method, provide more detailed and reliable data than those with the φ angle fixed. Diffraction studies show that the influence of thermal fatigue on the lattice parameters of the alloy is very limited. The stress analysis reveals that triaxial elastic hydrostatic stress plays a major role during thermal fatigue. The magnitude of the macrostress increases with the fatigue cycles, with the stress of the γ phase increasing more significantly than that of the γ' phase, and becoming fragile after many cycles. The changes in the microstrain are dependent on the reflection planes. The microstrains at the center of the sample are released by the thermal fatigue in comparison with those at the outlying locations, which has been attributed to the advance of the dislocation slips.

PACS: 62. 40. +i, 28. 20. Cz

The single crystal (SC) Ni based superalloys owe high-temperature strength, in the absence of grain boundaries and precipitation hardening, to a high volume fraction of ordered cuboidal γ' particles in the face-centered cubic (fcc) γ matrix. The lattice mismatch affected by difference in thermal expansion coefficients of the γ and γ' phases in the SC superalloy during temperature change is a source of internal stress, and will affect the thermal fatigue (TF) behavior of the alloy.[1−5] X-ray and neutron diffraction have been successfully applied to evaluate the stress and strain states of various superalloys.[6−8] The TF of the polycrystalline superalloys has been studied using the neutron diffraction technique,[9] but TF study of SC superalloys is still rare.

Some interesting results have been obtained in our recent measurements of the thermomechanically fatigued (TMF) SC superalloy in SALSA. The initial analysis shows a general trend of increasing internal stress and microstrain with the number of TMF cycles.[10] A tetragonal distortion of the γ and γ' phases associated with the cycling deformation is observed. The associated defect development during cycling is also revealed by further TEM studies.[11]

The samples are SC DZ125L superalloy (wt%): 8.9Cr, 9.6Co, 6.6W, 2.1Mo, 10.6(Al+Ti+Ta) and Ni in balance, with a growth direction of [001]. The volume ratio of the γ and γ' phases is 40:60. The sample is a short cylinder 14 mm in diameter and 16 mm in length with a hanger hole on the top arch. During each TF cycle, the sample is hoisted up into the furnace at 900°C in air for 7 min, and down into water for cooling for 1 min. Two TF samples of 100 and 1000 cycles, and a standard sample without TF treatment are prepared for the measurements.

A neutron wavelength of 1.55 Å, 2θ values of {311} planes at about 92°, {220} planes at about 76° and {400} planes at about 119° are used for the measurements.[12] In order to reduce the wavelength divergence across the primary beam and avoid the peak clipping effect, a gauge volume of 1.2 mm × 1.2 mm × 2 mm is defined by the oscillating horizontal radial collimators and the vertical slits. In this case, the radial collimators facilitate the use of a position-sensitive detector while maintaining accurate spatial definition. At least six planes are measured at the center, 3 mm away from the center (3AC) and 6 mm away from the center (6AC) along the axis of the sample to reveal the stress state at these locations.

The x-ray study of the microstructure of the Ni based superalloy CMX-4 and rocking-curve analysis by Lang *et al.*[13] indicated that the technically grown SC superalloys have a non-negligible mosaic spreading. In previous measurements, each (hkl) reflection in the oriented SC sample was optimized by a $\chi-\varphi$ mapping procedure,[8,9] and the mosaic spreading of the sample (mutual misorientations between dendrites) is overlooked.[14] In this work, an additional measurement is adopted such that the φ angle is unceasingly oscillated around the central axis with the angle range corresponding to the spreading of the $\{hkl\}$ plane during the measurement.

The stress and strain state of the location is obtained from the position and broadening of the reflection profile based on the relevant fitting procedure. As shown in Fig. 1, most individual reflections are similar to the patterns shown in Figs. 1(a) and 11(b) with Gaussian distribution profiles. Acceptable agreement

**To whom correspondence should be addressed. Email: guangaisun_80@163.com

can be achieved either by one peak fitting or by double peak fitting to deconvolve the γ and γ' peaks. The dependence of the scattering lengths on the element in connection with different compositions of the phases leads to an intensity ratio of $I_{\gamma'}/I_{\gamma} = 1.05$ for the constraint of double peak fitting. One peak fitting is more reliable as it has fewer constraints (see Fig. 1(a)). However, some reflections fit better by the deconvolution of the γ and γ' peaks (see Fig. 1(b)). The discussions are primarily based on one peak fitting results, unless explained. The detailed analysis has been described elsewhere.[10,15]

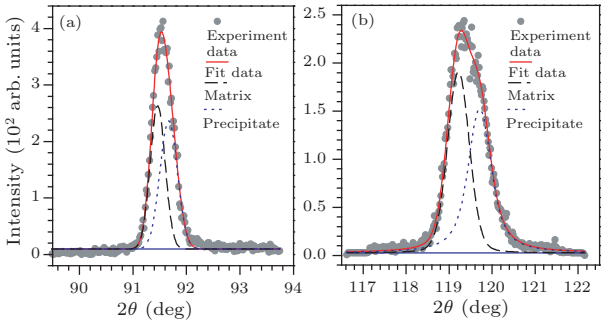

Fig. 1. An example of the fit of the diffraction pattern including the two γ and γ' phases based on the intensity ratio: (a) the $(1\bar{1}\bar{3})$ plane of standard sample center, (b) the (400) plane of TF1000 cycles center.

Figure 2 shows the diffraction patterns of some {311} planes measured by the φ oscillating method. Some abnormality at the root of the individual peak can be observed in the diffraction patterns, such as that on the $(13\bar{1})$ plane of TF 1000-cycle sample. Detailed examination as shown in Fig. 2(b) indicates that such abnormality has only occurred in the pattern collected with the φ oscillating method. These abnormalities could be caused by scattering of some large irregular misorientations between dendrites or subgrains in the interdendritic regions, and thus indicate the significant imperfections of the SC superalloy. As there are usually a few crystal planes contributing to the reflection and the peak positions are easily affected by the dislocation and vacancy in SC measurements, the reflections collected by the φ oscillating method provide an average of more planes with similar orientation in a location, thus will be more reliable for the stress state of the region.

Table 1 lists the full width at half maximum (FWHM) of standard and TF100 samples measured by φ oscillating and φ fixed methods, respectively. In comparison of different crystal plane groups, the $\varphi_{\rm osc}/\varphi_{\rm fix}$ FWHM increases with 2θ, and the average value of FWHM obtained by φ oscillating are all larger than that from φ fixed. These results indicate that the mosaic spreading has obviously contributed to the scattering divergences. A remarkable difference $\varphi_{\rm osc} - \varphi_{\rm fix}$ of the FWHM values indicates that the dendritic structure and the mutual misorientations between the dendrites are distributed anisotropically among the crystal planes.[16] Therefore, the following results have been provided by the data collected by the φ oscillating method.

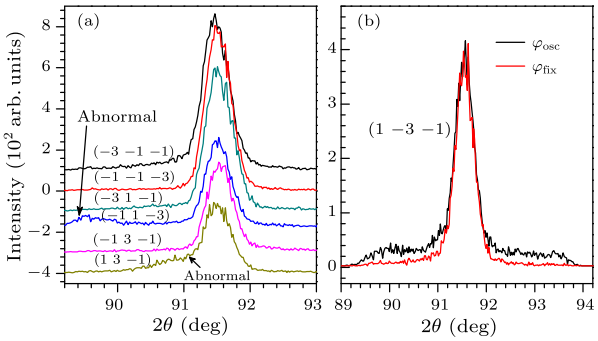

Fig. 2. Diffraction profiles of the {311} planes: (a) obtained at 6AC of TF 1000 cycle sample using the φ oscillating method, (b) from the standard sample center using the φ oscillating and fixed methods.

Table 2 illustrates the lattice parameters derived from the least square fitting of all relevant reflections, and the values of lattice parameter a (100)/(010) in the [100]/[010] direction and c (001) parallel to the [001] have been displayed, respectively, to demonstrate the effect of tetragonal lattice distortion. The lattice parameters of the γ and γ' phases are global averages over the entire gauge volume, and may differ from the values determined by convergent beam electron diffraction (CBED) measurements, which involve only the local microstructural information. Earlier studies did not distinguish the difference between the local and the global measurements.[17] Moreover, due to the coherency matching between γ' precipitates and the γ matrix, the lattice symmetry may in fact change near the γ'/γ interface. This change of symmetry may be due to dilation/contraction, as well as to angular distortions of the crystal lattice.

Table 1. Average of FWHM of different samples from φ oscillating and fixed methods.

Crystal planes	FWHM of standard sample (deg)			FWHM of TF 100 cycles sample (deg)		
	$\varphi_{\rm osc}$	$\varphi_{\rm fix}$	$\varphi_{\rm osc} - \varphi_{\rm fix}$	$\varphi_{\rm osc}$	$\varphi_{\rm fix}$	$\varphi_{\rm osc} - \varphi_{\rm fix}$
{220}	0.4229	0.3643	0.0576	0.3925	0.3643	0.0282
{311}	0.4544	0.4431	0.0113	0.4574	0.4552	0.0022
{400}	0.8537	0.7515	0.1022	0.9032	0.7977	0.1055

Table 2. Lattice parameters determined by the φ oscillating method.

Lattice parameter	TF0	TF100	TF100 (6 mm AC)	TF1000	TF1000 (3 mm AC)	TF1000 (6 mm AC)
a(Å)	3.5868(6)	3.5874(6)	3.5881(1)	3.5885(2)	3.5883(1)	3.5889(8)
c(Å)	3.5866(5)	3.5869(6)	3.5880(5)	3.5875(6)	3.5874(3)	3.5866(6)

As shown in Table 2, along with the increasing TF cycles, the lattices of the SC superalloy appear to have increased and distorted slightly, with the lattice parameter a increasing more than c. For the sample with most TF cycles (1000), the lattice parameters have also shown sign of dependence on the location of the sample, with the lattice parameter close to the surface (6AC) distorted more than those measured at the center and 3AC locations. This dependence is likely to be caused by the thermal stress variance during the TF process. During the temperature change, the surface of the sample will be the most affected. However, unlike those observed in the TMF samples,[18] the detected lattice parameter changes in the TF samples are only slightly larger than the standard deviations of the measurements. Therefore, the TF has only a very limited influence on the average lattice parameters, which is consistent with the fact that there is no external stress applied to the samples during the TF process.

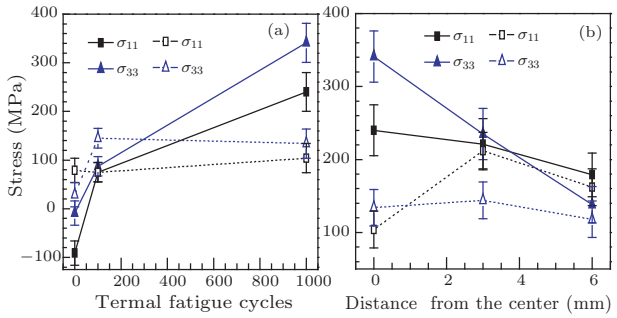

Fig. 3. Variation of the stress (a) with TF cycles, (b) with different locations of TF 1000 cycle sample. The solid lines show the γ phases and the dotted lines are for the γ' phase.

As indicated above that the changes in the lattice parameters are subject to the existence of internal stress, and the internal stress state of the samples are calculated and examined. Table 3 lists the macroscopic stress of the samples, where σ_{33} is along the axial direction, σ_{11} and σ_{22} are on the cross section, and σ_{11} and σ_{22} are equivalent, σ_{13} and σ_{23} are the same. As shown in the table, the normal stresses of σ_{11}, σ_{22} and σ_{33} after TF have become positive, and increase with TF cycles, which may be due to substructure variation such as the gradual loosing of the coherence between the phases. The stresses at the 6AC location are slightly larger than those at the center. However, all the normal stresses have been larger than the shear stresses, which indicates that the elastic hydrostatic stresses play more important roles than the deviatoric stresses during the TF process.

As the normal stresses are predominant in TF, the normal stresses of the γ and γ' phases obtained by doublet fitting the profiles have been exhibited, respectively (see Fig. 3). As shown in Fig. 3(a), at the initial stage, the γ matrix is compressed and the γ' precipitates are stretched, which is consistent with the internal stress state of the two phases calculated from finite element analysis.[19] However, along with the advance of TF, the internal stresses of the γ matrix have increased considerably more than those of the γ' precipitates. Therefore, after many cycles of TF (TF1000), the internal stresses of the γ matrix have become higher than that of the γ' precipitate, and the stresses of both the γ matrix and the γ' precipitates have become positive. However, for the interphase stress, the γ matrix has become stretched and the γ' precipitates compressed. This means that the advance of the TF has put the γ matrix into a more fragile state of tensile stress for cracking. However, although there are some differences between the stress of σ_{11} and σ_{33}, their trends are very similar. This is due to the fact that the differences between σ_{11} and σ_{33} are basically caused by crystal growth orientation and geometrical factors, and are not related to the external stress. As shown in Fig. 3(b), after 1000 cycles of TF, the difference of the internal stress between different locations has been prompted. Although the macroscopic stresses at 6AC are greater than that at the center location (see Table 3), the increasing differences between the γ matrix and the γ' precipitates at the center are obvious. It is known that the elastic moduli of an Ni-based superalloy and its isolated phases are dependent on temperature. In general, Young's modulus of the γ matrix is larger than that of the γ' precipitates at low temperature, but the relationship changes at high temperatures of about 750°C depending on the alloys.[20] The temperature dependence of the Young's modulus of the superalloy is not linear and is higher than in its isolated phases.[21] Frequent stress variations on the interface caused by the modulus changes of the two phases under the TF process will lead to a permanent change in the microstructure of the alloys, and thus result in the internal stress changes. The dependences of the internal stresses on both the TF cycles and the sample locations in Fig. 3 are likely to be caused by the above scenario.

Table 3. Macrostress information derived from the $\varphi_{\rm osc}$ neutron diffraction measurements.

TF cycles	0	100	1000	1000 (6AC)
Stress (MPa)	$\begin{bmatrix} -9 & -21 & 15 \\ -21 & -9 & -17 \\ 15 & -17 & 13 \end{bmatrix}$	$\begin{bmatrix} 64 & -3 & -84 \\ -3 & 64 & 41 \\ -84 & 41 & 120 \end{bmatrix}$	$\begin{bmatrix} 140 & -43 & -24 \\ -43 & 140 & 7 \\ -24 & 7 & 160 \end{bmatrix}$	$\begin{bmatrix} 190 & 93 & -18 \\ 93 & 190 & 32 \\ -18 & 32 & 140 \end{bmatrix}$

Figure 4 exhibits the trend of the development of the broadening of the reflections obtained from the measurements. As shown in Fig. 4(a), the FWHMs of the {311} planes is higher and stable, whereas that of the {220} planes are smaller and change during the TF process. It is interesting to note that the FWHMs of the {220} planes have decreased rather than be increased by the TF. A similar but reversible phenomenon was observed by an in-situ diffraction measurement at high temperature, which has been attributed to the above-mentioned change of elastic modulus at different temperatures.[22] However, in our case, the decrease in FWHM has been observed as a residual effect at room temperature. The observed dependence of the FWHM on the reflection planes reflects the anisotropic nature of the microstrains, which is often associated with the existence of dislocation defects. However, although the observed anisotropic FWHM is consistent with the dislocation model, the dependence of the resolution of the instrument on the scattering angle complicates the relation. Therefore, we will focus the discussion on the relation between the microstrains and TF cycles. The octahedral ⟨110⟩ {111} slip is the primary slip system in the fcc structure. The dislocations pile up or release on the associated {220} planes and lead to relevant microstrain changes, whereas other planes, not associated with the slip system such as {311}, will hardly be affected. As mentioned above, the stress variations on the γ/γ' interface caused by the TF process could prompt the ⟨110⟩ {111} slip, therefore reduce the dislocation densities and release the strains on the {220} planes.[23]

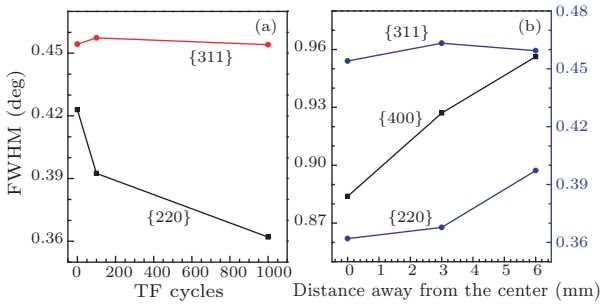

Fig. 4. Relation between the average line width of the reflection profile and (a) the TF cycles measured at the center, (b) the location of the TF1000 cycle sample, where the scale on the left is for the {220} and (311) planes, and the scale on the right is for the {400} planes. The standard deviation of the measured values is 0.01°.

However, as shown in Fig. 4(b), the relation between the FWHM and the location of the TF1000 sample has also shown a similar dependence on the reflection planes. In general, the FWHM increased with the distance from the center. However, the change on the {400} and {220} planes are significantly greater than that on the {311} planes. These changes may also be explained by the effects of dislocations on the octahedral and cube slip systems, since both {400} and {220} planes are the associated dislocation planes in these systems. The dependence of the FWHM on the location of the sample reflects the distribution of the defects in the samples. The macrostresses on the outlying locations of the sample are greater than those on the center, and will be more effective in creating dislocations. However, it has been observed that the γ' precipitates during cooling from the aging temperature not only introduce a misfit strain, but also change at the same time, in a complex fashion, the matrix composition.[24,25] Such an effect can also develop an anisotropic distribution of microstrains.

In summary, The measurements using the φ angle oscillating method reveal some large irregular misorientations between the dendrites or subgrains in the interdendritic regions. Slight expansion and distortion of the average lattice parameters in TF samples are observed. However, the influences of the TF on the lattice parameters of the alloy are very limited. The stress analysis shows that during TF process, the triaxial elastic hydrostatic stress plays a predominant role, in comparison with that of the deviatoric stress. The magnitude of the macrostress has increased with the TF cycles, and become greater at the outlying location of the sample. The stress of the γ phase increases more significantly than that of the γ' phase, and changes from the compressive state to the tensile state. The microstrains are dependent on the reflection planes and distribute anisotropically in the TF samples. The microstrains are released at the center of the sample, but accumulate at the outlying positions during the TF process.

References

[1] Lin Y C et al 2003 *J. Mater. Proc. Technol.* **138** 22
[2] Biermann H et al 1995 *Scripta Metall. Mater.* **32** 1405
[3] Kuhn H A et al 1991 *Acta Metall. Mater.* **39** 2783
[4] Bhattachar V S 1995 *Int. J. Fatigue* **17** 407
[5] Yang J X et al 2006 *Rare Met.* **25** 202
[6] Menig R et al 2001 *Scripta Mater.* **45** 977
[7] Muller L et al 1992 *Scripta Metall. Mater.* **26** 1297
[8] Holden T M et al 1995 *Physica* B **213–214** 793
[9] Lukas P et al 2000 *Mater. Sci. Forum* **321–324** 1046
[10] Wu E et al 2008 *J. Phys: Condens. Matter* **20** 104255
[11] Wu E, Li J C et al 2008 *Metall. Mater. Trans.* A **39** 3141
[12] Sun G A et al 2009 *Chin. Phys. Soc.* **58** 2549
[13] Lang C et al 1995 *Acta Metall Mater.* **43** 1751
[14] Glatzel U et al 1994 *Scripta Metall. Mater.* **31** 285
[15] Ma S et al 2003 *Scripta Mater.* **48** 525
[16] Huang E W et al 2007 *Int. J. Plasticity* **24** 1440
[17] Gilles R et al 2006 *Acta Mater.* **54** 1307
[18] Marty B et al 1997 *Acta Mater.* **45** 791
[19] Glatzel U et al 1994 *Scripta Metall. Mater.* **31** 291
[20] Sieborger D et al 2001 *Mater. Sci. Engin.* A **298** 26
[21] Ichitsubo T et al 2003 *Acta Mater.* **51** 4863
[22] Darowski N et al 2005 *J. Phys. D: Appl. Phys.* **38** A200
[23] Westbrooke E F et al 2005 *Acta Mater.* **53** 2137
[24] Fahrmann M et al 1996 *Mater. Sci. Engng.* A **210** 8
[25] Zrnik J et al 2004 *Mater. Sci. Engng.* A **387–389** 728